Semiclassical treatment of photon cascades in nuclei

Jørgen Randrup[1] and Thomas Døssing[2]
[1]*Nuclear Science Division, Lawrence Berkeley National Laboratory, Berkeley, California 94720, USA*
[2]*Niels Bohr Institute, University of Copenhagen, Copenhagen DK-2100, Denmark*

We present a simple semiclassical treatment of photon cascades, suitable for use in nuclear fission simulation codes. The approximation is here developed for $E1$ and $E2$ transitions and its quality is illustrated for a variety of two-photon cascades. Implementation of the treatment into Monte Carlo simulations would make it possible to address photon correlation observables quantitatively.

I. INTRODUCTION

Low-energy fission leads to primary fragments that each have about a dozen MeV of excitation and half a dozen units of angular momentum, on average. The fragments, after possible neutron evaporation, deexcite by sequential photon emission. The associated emission patterns may reveal interesting aspects of the fission process, such as the directions of the fragment angular momenta and their mutual correlations. In particular, seminal measurements of the angular distribution from collective transitions have shown that the angular momenta are preferentially perpendicular to the fission direction [1,2] and recent experiments, also involving rotational transitions, suggest that their magnitudes are largely uncorrelated [3].

The physical mechanisms responsible for the fission-fragment angular momenta are currently a topic of active research. Although many recent correlation experiments have helped to illuminate the issue [3–10], a variety of mechanisms are being advocated [3,11–20]. There is thus a need for careful calculation of the observable consequences of the various models proposed and photon correlation measurements may be particularly revealing.

The relevant fission observables are most conveniently calculated by means of event-by-event Monte Carlo simulations which yield large samples of complete final states from which any distribution and correlation can subsequently be extracted (see, for example, Ref. [21]). Several treatments have been developed for this purpose, most notably CGMF [22,23], FREYA [24,25], FIFRELIN [26], and GEF [27]. These simulation codes differ in various ways, including how the fragment deexcitation processes are treated. For example, CGMF invokes a considerable degree of nuclear structure information within the Hauser-Feshbach framework, but it does not keep track of directional information through a cascade. By contrast, FREYA treats the nuclear properties in a farily generic way but keeps careful track of all conserved quantities throughout, including the correlated directions of the fragment angular momenta. FIFRELIN also uses the Hauser-Feshbach framework and its treatment of the photon cascades has recently been augmented with a statistical tensor formalism that makes it possible to calculate correlation observables [28].

Directional correlations between the photons emitted during a decay cascade arise because each emitted photon carries some angular momentum and that affects the direction of the angular momentum of the corresponding daughter nucleus, thereby influencing the angular distribution of the next photon emitted. The inclusion of such "spin-recoil" effects, while highly interesting, is complicated to accomplish in an exact quantal treatment. We have therefore developed a simple semiclassical treatment that includes the successive changes in the nuclear spin direction and makes it practical to simulate the correlated photon emissions in a Monte Carlo approach.

Section II describes how the approximate treatment can be carried out for $E1$ and $E2$ transitions and Sec. III subsequently illustrates how well it works for a variety of two-photon cascades. Our concluding remarks are presented in Sec. IV.

II. TREATMENT

In fission simulation models such as FREYA the primary fission fragments have classical angular-momentum vectors that have been sampled from specific correlated distributions prescribed by the underlying physical model. These fragments (may) then evaporate neutrons, leading to prompt product nuclei that are typically excited by $\approx$5 MeV and their angular momenta, although modified by evaporation, are still mutually correlated (both individually with respect to the fission direction and mutually).

We assume that each such product nucleus can be represented quantally as a maximally aligned state, with the initial alignment direction being that of the postevaporation classical angular-momentum vector. It is described below how the semiclassical treatment applies to a single step in the subsequent photon deexcitation cascade. The approximation procedure can then be applied for each emission throughout the cascade.

Thus it is generally assumed that the nucleus, before emitting the photon, has a definite spin magnitude J (as well as a definite excitation energy E) *and* that its spin is maximally

aligned along some direction, i.e., its quantum state has the form $|\mathcal{N}\rangle = |\alpha; J, M = J\rangle$ when that direction is used as the quantization axis. Furthermore, the final nuclear state, after the emission, $|\mathcal{N}'\rangle$, has also a definite spin magnitude J' (and a definite excitation E') *and* it is maximally aligned along some (generally different) direction depending on the emission direction of the photon (and the multipolarity of the transition).

To describe the treatment in detail, we introduce the initial reference system $\mathcal{S}(\hat{\mathbf{x}}, \hat{\mathbf{y}}, \hat{\mathbf{z}})$ that is oriented such that $\hat{\mathbf{z}}$ points along the alignment direction of the initial (mother) nucleus; we may then write $|\mathcal{N}\rangle = |\alpha; J, J\rangle_{\hat{z}}$. In the energy region of interest, the level spacings are larger than the decay widths and decays to different nuclear levels can then be considered as being mutually incoherent. A decay of multipolarity λ therefore leads to a nucleus-photon state having the following form,

$$|f\rangle_{J',h} = \sum_{\mu=-\lambda}^{\lambda} \langle J', M'; \lambda, \mu | J, J\rangle |\alpha'; J', M'\rangle |\lambda; \mu, h\rangle, \quad (1)$$

where J' is the angular momentum of the daughter level and $h = \pm 1$ is the helicity of the emitted photon. Furthermore, $|\alpha'; J', M'\rangle$ is a nuclear angular-momentum eigenstate (with respect to $\hat{z}$) and $|\lambda, \mu h\rangle$ denotes the state of a photon having the total angular momentum λ, the projection μ on $\hat{z}$, and the helicity h. In this state, the amplitude for the photon to be moving in the direction $\hat{\boldsymbol{\omega}} = \boldsymbol{p}/\varepsilon = (\theta, \phi)$ is

$$\langle \hat{\boldsymbol{\omega}} | \lambda; \mu, h\rangle = \langle \lambda, \mu | e^{i\phi \hat{J}_z} e^{i\theta \hat{J}_y} | \lambda, h\rangle = d^{\lambda}_{\mu,h}(\theta) e^{i\mu\phi}, \quad (2)$$

where the Wigner d functions relevant here are

$$d^1_{0,h}(\theta) = \frac{h}{\sqrt{2}} \sin\theta, \quad d^1_{\pm 1,h}(\theta) = \frac{1}{2}(1 \pm h\cos\theta), \quad (3)$$

$$d^2_{0,h}(\theta) = -\sqrt{\frac{3}{2}} h \sin\theta\cos\theta, \quad (4)$$

$$d^2_{1,h}(\theta) = \frac{1}{2}(\cos\theta + h\cos 2\theta)\sin\theta, \quad (5)$$

$$d^2_{2,h}(\theta) = -\frac{1}{2}(1 \pm h\cos\theta)\sin\theta. \quad (6)$$

Thus, for each J' and h, the emitted photon and the daughter nucleus are generally in an entangled state $\langle \hat{\boldsymbol{\omega}} | f\rangle$, with the nucleus being left in a different superposition of rotational substates $|\alpha'; J', M'\rangle$ for each photon emission direction $\hat{\boldsymbol{\omega}}$. It follows that the expectation value of the angular momentum in the nuclear daughter state, $\underline{\boldsymbol{J}}' = (\underline{J}'_x, \underline{J}'_y, \underline{J}'_z)$, generally has the following form:

$$\underline{\boldsymbol{J}}'(\hat{\boldsymbol{\omega}}) = (\underline{J}'_{\perp}(\theta)\cos\phi,\ \underline{J}'_{\perp}(\theta)\sin\phi,\ \underline{J}'_z(\theta)). \quad (7)$$

This means that the (mean) angular-momentum vector of the daughter nucleus, $\underline{\boldsymbol{J}}'$, is *tilted* relative to that of the mother nucleus, $\underline{\boldsymbol{J}} = J\hat{z}$. The azimuthal direction of the tilted vector is either opposite of ϕ (for $h = +1$) or equal to ϕ (for $h = -1$). Thus the tilting angle $\chi(\theta)$, which is determined by $\tan\chi = \underline{J}'_{\perp}(\theta)/\underline{J}'_z(\theta)$, can have either sign.

The principal approximation in the present semiclassical treatment is to replace the actual nuclear daughter state, $\langle \hat{\boldsymbol{\omega}} | f\rangle$, by a state that is maximally aligned along $\underline{\boldsymbol{J}}'(\hat{\boldsymbol{\omega}})$, i.e., it has the form $|\alpha'; J', J'\rangle$ in a reference system $\mathcal{S}'(\hat{\boldsymbol{x}}', \hat{\boldsymbol{y}}', \hat{\boldsymbol{z}}')$ that has its polar axis $\hat{\boldsymbol{z}}'$ directed along $\underline{\boldsymbol{J}}'(\hat{\boldsymbol{\omega}})$, i.e., $|\mathcal{N}'(\hat{\boldsymbol{\omega}})\rangle = |\alpha'; J', J'\rangle_{\hat{\boldsymbol{z}}'}$.

III. ILLUSTRATIONS

The quality of the semiclassical approximation introduced above can be illustrated by cascades of two successive $E\lambda$ emissions. As stated above, for each two-photon cascade it is assumed that the nucleus is initially in a maximally aligned quantum state $|\mathcal{N}\rangle = |\alpha; J, J\rangle$. The correlation effects decrease as J is increased. Therefore, in order to better bring out the differences, the illustrations are made for relatively small values of J.

For each type of cascade, the exact expression for the joint directional distribution of the two emitted photons, $P_{12}(\hat{\boldsymbol{\omega}}_1, \hat{\boldsymbol{\omega}}_2) = d^2N_{12}/d^2\hat{\boldsymbol{\omega}}_1 d^2\hat{\boldsymbol{\omega}}_2$, can be derived in an elementary manner by successive use of Eq. (1).

The approximate joint angular distribution is obtained by Monte Carlo simulation. The emission direction of the first photon, $\hat{\boldsymbol{\omega}}_1 = (\theta_1, \phi_1)$, is sampled from the appropriate angular distribution, $P_1(\hat{\boldsymbol{\omega}}_1)$. The associated tilting angle $\chi(\theta_1)$ is then calculated (see below). That determines the alignment direction $\hat{\boldsymbol{z}}'$ of the nuclear daughter state for which the procedure is then repeated, yielding the emission direction $\hat{\boldsymbol{\omega}}_2 = (\theta_2, \phi_2)$ of the second photon (as well as the alignment direction $\hat{\boldsymbol{z}}''$ of the nuclear granddaughter state which is not needed here). For each particular type of cascade, a large sample of such two-photon emissions is generated and the observables of interest can then be extracted by suitable binning.

The individual angular distributions of the two photons are related to the joint distribution by projection,

$$P_1(\hat{\boldsymbol{\omega}}_1) = \int d^2\hat{\boldsymbol{\omega}}_2 P_{12}(\hat{\boldsymbol{\omega}}_1, \hat{\boldsymbol{\omega}}_2), \quad (8)$$

$$P_2(\hat{\boldsymbol{\omega}}_2) = \int d^2\hat{\boldsymbol{\omega}}_1 P_{12}(\hat{\boldsymbol{\omega}}_1, \hat{\boldsymbol{\omega}}_2). \quad (9)$$

The exact expressions for $P_1(\theta_1)$ and $P_2(\theta_2)$ can readily be derived from the exact joint distribution, while the approximate distributions can be obtained by event-by-event binning of the sampled directions θ_1 and θ_2.

The approximate treatment is obviously exact for the angular distribution of the first photon, $P_1(\hat{\boldsymbol{\omega}}_1)$, provided that the initial state is in fact maximally aligned, so only the angular distribution of the second photon, $P_2(\hat{\boldsymbol{\omega}}_2)$, needs to be examined.

It is of particular interest to determine how well the approximate treatment reproduces the correlations between two subsequent emission directions. To illustrate this crucial feature, we consider the distribution of the opening angle ψ_{12} between the two emission directions $\hat{\boldsymbol{\omega}}_1$ and $\hat{\boldsymbol{\omega}}_2$, where

$$\cos\psi_{12} = \hat{\boldsymbol{\omega}}_1 \cdot \hat{\boldsymbol{\omega}}_2 = \cos\theta_1\cos\theta_2 + \sin\theta_1\sin\theta_2\cos\phi_{12}, \quad (10)$$

with $\phi_{12} \equiv |\phi_1 - \phi_2|$. The exact distribution of ψ_{12} is given by

$$P_{\psi}(\psi) = \int d^2\hat{\boldsymbol{\omega}}_1 d^2\hat{\boldsymbol{\omega}}_2 \delta(\psi_{12} - \psi) P_{12}(\hat{\boldsymbol{\omega}}_1, \hat{\boldsymbol{\omega}}_2), \quad (11)$$

while the approximate distribution can be obtained by event-by-event binning of ψ_{12}.

A. Sequential $E1$ emission

We consider first two sequential $E1$ emissions during which the magnitude of the nuclear spin evolves as $J \to J' \to J''$. In each individual emission, the magnitude may change by up to one unit, so there are a total of nine different cascade types, each one characterized by the particular combination of the spin changes, and they are considered in turn below.

1. E1-E1: $J' = J - 1$

For these three cascade types, the first transition is stretched and only $\mu = 1$ contributes in Eq. (1). Thus the exact nuclear daughter state is maximally aligned along the initial alignment direction $\hat{\boldsymbol{z}}$,

$$\langle \hat{\boldsymbol{\omega}}_1 | \mathcal{N}' \rangle^{E1}_{J-1,h_1} \;=\; |\alpha'; J-1, J-1\rangle_{\hat{\boldsymbol{z}}}, \tag{12}$$

and the angular distribution of the first photon has a simple form, $P_1(\theta_1) \sim d^1_{1,h_1}(\theta_1)^2$. Furthermore, because $\underline{\boldsymbol{J}}' = (0, 0, J')$ we have $\underline{J}'_\perp = 0$, so the tilting angle vanishes, $\chi = 0$. The treatment is then exact also for the second emission, so there is no need to check these cases.

2. E1-E1: $J' = J$

For these cascades both $\mu = 0$ and $\mu = 1$ in Eq. (1) contribute for the first emission, so the daughter state has the form

$$\langle \hat{\boldsymbol{\omega}}_1 | \mathcal{N}' \rangle^{E1}_{J,h_1} = h_1 c_0(\theta_1) |\alpha'; J, J\rangle - c_1(\theta_1) e^{i\phi_1} |\alpha'; J, J-1\rangle, \tag{13}$$

with $c_0^2 + c_1^2 = 1$ and

$$c_0 \sim \left[\frac{J}{J+1}\right]^{\frac{1}{2}} h_1 d^1_{0,h_1}(\theta_1), \quad c_1 \sim \left[\frac{1}{J+1}\right]^{\frac{1}{2}} d^1_{1,h_1}(\theta_1). \tag{14}$$

The angular distribution of the first photon is then a mix of $|\alpha; J, J\rangle \to |\alpha'; J, J\rangle$ and $|\alpha; J, J\rangle \to |\alpha'; J, J-1\rangle$,

$$P_1(\hat{\boldsymbol{\omega}}_1) \sim \frac{J}{J+1} d^1_{0,h_1}(\theta_1)^2 + \frac{1}{J+1} d^1_{1,h_1}(\theta_1)^2. \tag{15}$$

Furthermore,

$$\underline{J}'_\perp(\theta_1) = -h_1 \sqrt{2J} c_0 c_1, \quad \underline{J}'_z(\theta_1) = J c_0^2 + (J-1) c_1^2, \tag{16}$$

so the tilting is away from the azimuthal emission direction when the photon has positive helicity and towards the azimuthal emission direction when it has negative helicity, as might be intuitively expected.

The angular distribution of the second photon in $E1$ cascades where the first emission leaves the nuclear spin unchanged, $J' = J$, is illustrated in Fig. 1 for $J'' - J' = -1, 0, +1$. For each cascade type, the result of the semiclassical treatment is compared with the exact quantal polar profile.

Generally, the exact directional distribution is very well reproduced by the semiclassical treatment. The largest differences amount to slight overshoots (by a few percent) in the polar regions where the yield is suppressed by the geometric factor $\sin\theta_2$,

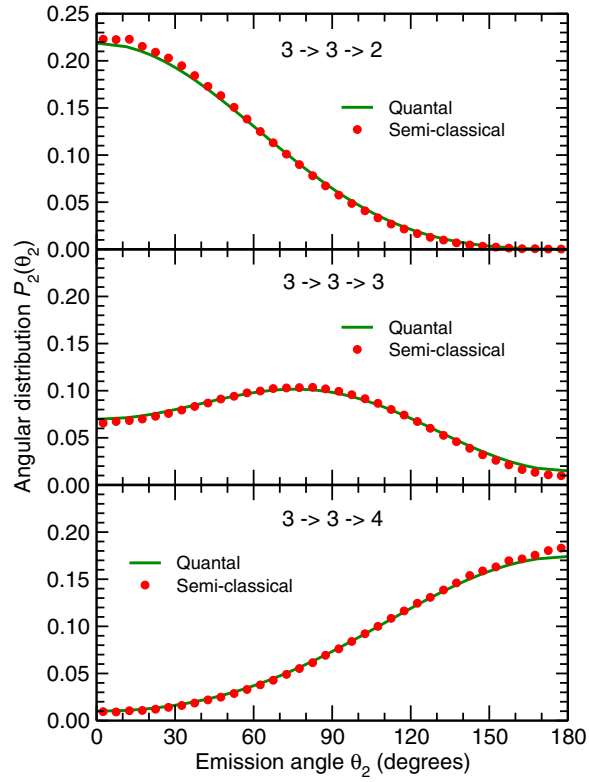

FIG. 1. The angular distribution of the second $E1$ photon, $P_2(\hat{\boldsymbol{\omega}}_2)$, for the three cascade types where the first $E1$ emission does not change the nuclear-spin magnitude, $J' = J$, calculated for $h_1, h_2 = 1$. Solid (green) curve: the exact quantal distribution; solid (red) circles: the semiclassical simulation.

The corresponding distributions of the opening angle ψ_{12} between the two emission directions $\hat{\boldsymbol{\omega}}_1$ and $\hat{\boldsymbol{\omega}}_2$ are shown in Fig. 2. The semiclassical approximation is seen to be generally rather good. The largest deviations occur for $\psi_{12} \approx 0$ and $\psi_{12} \approx 180^\circ$ where the yield is small due to the geometric $\sin\psi_{12}$ weight.

Also shown is how the distribution of ψ_{12} would look if the two emissions were mutually independent, i.e., if the joint distribution factorizes, $P_{12}(\hat{\boldsymbol{\omega}}_1, \hat{\boldsymbol{\omega}}_2) = P_1(\hat{\boldsymbol{\omega}}_1) P_2(\hat{\boldsymbol{\omega}}_2)$. It is noteworthy that the qualitative appearance of the uncorrelated ψ_{12} distribution is opposite of the exact result when the second emission is stretched or antistretched, so in these cases the spin recoil has a particularly significant effect and it is important to take account of the inherent correlations between successive emission directions.

3. E1-E1: $J' = J + 1$

For these three cases, the first transition is antistretched. Then all three terms in Eq. (1) contribute and the nuclear daughter state has the form

$$\begin{aligned}\langle \hat{\boldsymbol{\omega}}_1 | \mathcal{N}' \rangle^{E1}_{J+1,h_1} = {} & c_-(\theta_1) e^{-i\phi_1} |\alpha'; J+1, J+1\rangle \\ & - h_1 c_0(\theta_1) |\alpha'; J+1, J\rangle \\ & + c_+(\theta_1) e^{i\phi_1} |\alpha'; J+1, J-1\rangle,\end{aligned} \tag{17}$$

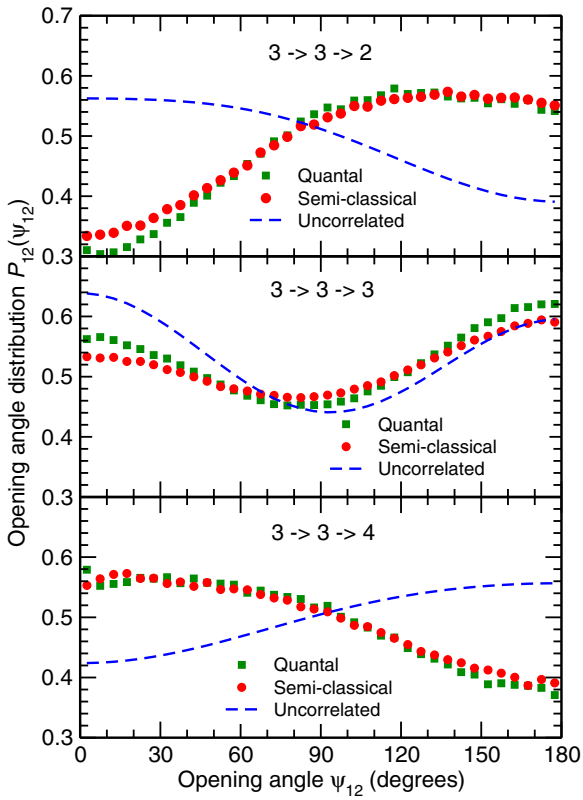

FIG. 2. The distribution of the opening angle between the emission directions of two sequential $E1$ photons, $P_\psi(\psi_{12})$, for the three cases where the first emission does not change the nuclear spin magnitude, $J' = J$, calculated for $h_1, h_2 = 1$. Solid (green) squares: sampling of the exact distribution; solid (red) circles: semiclassical sampling; dashed (blue) curve: uncorrelated emission.

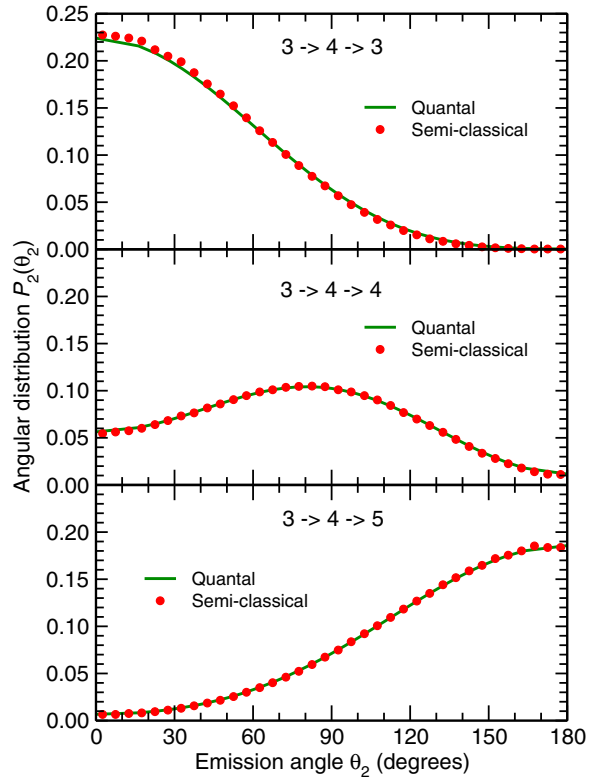

FIG. 3. The angular distribution of the second $E1$ photon, $P_2(\hat{\boldsymbol{\omega}}_2)$, for the three cases where the first $E1$ emission increases the nuclear spin, $J' = J + 1$, calculated for $h_1, h_2 = 1$. Solid (green) curve: exact distribution; solid (red) circles: semiclassical simulation.

with $c_-^2 + c_0^2 + c_+^2 = 1$ and

$$c_- \sim \left[\frac{2J+1}{2J+3}\right]^{\frac{1}{2}} d^1_{-1,h_1}(\theta_1) \geqslant 0, \tag{18}$$

$$c_0 \sim \left[\frac{2J+1}{(2J+3)(J+1)}\right]^{\frac{1}{2}} h_1 d^1_{0,h_1}(\theta_1) \geqslant 0, \tag{19}$$

$$c_+ \sim \left[\frac{1}{(2J+3)(J+1)}\right]^{\frac{1}{2}} d^1_{+1,h_1}(\theta_1) \geqslant 0. \tag{20}$$

Thus the angular distribution of the first photon has three components arising from $\Delta M = +1, 0, -1$,

$$P_1(\hat{\boldsymbol{\omega}}_1) \sim \frac{2J+1}{2J+3} d^1_{-1,h_1}(\theta_1)^2 + \frac{(2J+1) d^1_{0,h_1}(\theta_1)^2}{(J+1)(2J+3)} + \frac{d^1_{1,h_1}(\theta_1)^2}{(J+1)(2J+3)}. \tag{21}$$

The expectation value of the daughter spin then follows,

$$\underline{J'_\perp}(\theta_1) = -h_1 c_0 [\sqrt{2J+2}\, c_- + \sqrt{4J+2}\, c_+], \tag{22}$$

$$\underline{J'_z}(\theta_1) = (J+1)c_-^2 + J c_0^2 + (J-1)c_-^2. \tag{23}$$

Figure 3 shows the angular distribution of the second photon for the three $E1$ cascade types in which the first emission is antistretched, $J' = J + 1$. As in the three cases considered above (see Fig. 1), the semiclassical treatment provides an excellent approximation to the exact distribution of the second photon, with the largest deviations occurring in the (suppressed) polar regions and being hardly visible to the eye.

The corresponding distributions of the opening angle ψ_{12} are shown in Fig. 4. The accuracy of the semiclassical treatment is even better for these cases, being practically perfect for $J'' = J'$ and $J'' = J' + 1$, while the undulation amplitude is underestimated by about ten percent for $J'' = J' - 1$. As for the cases shown in Fig. 2, the inclusion of the directional correlations has a significant effect on $P_\psi(\psi_{12})$.

B. Sequential $E2$ emission

We consider here two sequential $E2$ emissions. In each individual emission, the nuclear-spin magnitude may in principle change by up to two units. However, only transitions that lower the angular momentum are of practical interest, $J > J' > J''$, so the spin may change only by -1 or -2 and there are then a total of just four different cascade types to be examined.

1. E2-E2: $J' = J - 2$

When the first transition is stretched, only $\mu = 2$ contributes in Eq. (1), so the daughter state remains

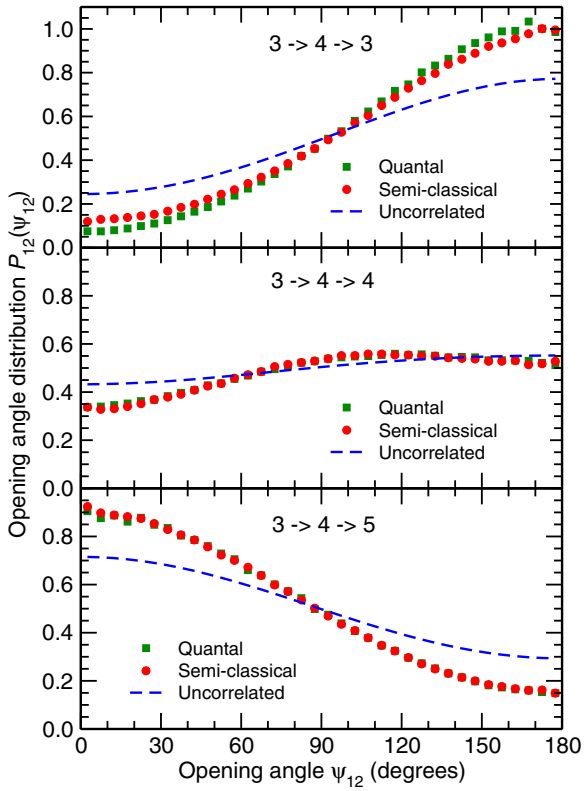

FIG. 4. The distribution of the opening angle between the emission directions of two sequential $E1$ photons, $P_\psi(\psi)$, for the three cases where the first emission is antistretched, $J' = J + 1$, calculated for $h_1, h_2 = 1$. Solid (green) squares: sampling of the exact distribution; solid (red) circles: semiclassical sampling; dashed blue curve: uncorrelated emission.

aligned,

$$\langle\hat{\boldsymbol{\omega}}_1|\mathcal{N}'\rangle^{E2}_{J-2,h_1} \;=\; |\alpha';J-2,J-2\rangle, \tag{24}$$

and the angular distribution of the first photon has a simple form, $P_1(\theta_1) \sim d^2_{2,h_1}(\theta_1)^2$. Furthermore, because then $\underline{J}'_\perp = 0$, there is no tilting, $\chi = 0$. The treatment is then exact also for the second emission, so there is no need to check these two cascade types.

2. E2-E2: $J' = J - 1$

For the cascades with $J' = J - 1$ both $\mu = 1$ and $\mu = 2$ in Eq. (1) contribute for the first emission, so the state of the daughter nucleus has the form

$$\begin{aligned}\langle\hat{\boldsymbol{\omega}}_1|\mathcal{N}'\rangle^{E2}_{J-1,h_1} \;=\; & c_1 e^{i\phi_1}|\alpha';J-1,J-1\rangle \\ & + c_2 e^{2i\phi_1}|\alpha';J-1,J-2\rangle,\end{aligned} \tag{25}$$

with $c_1^2 + c_2^2 = 1$ and

$$c_1 \sim \left[\frac{J-1}{J+1}\right]^{\frac{1}{2}} d^2_{1,h_1}(\theta_1), \tag{26}$$

$$c_2 \sim -\left[\frac{2}{J+1}\right]^{\frac{1}{2}} d^2_{2,h_1}(\theta_1) \;\geqslant 0. \tag{27}$$

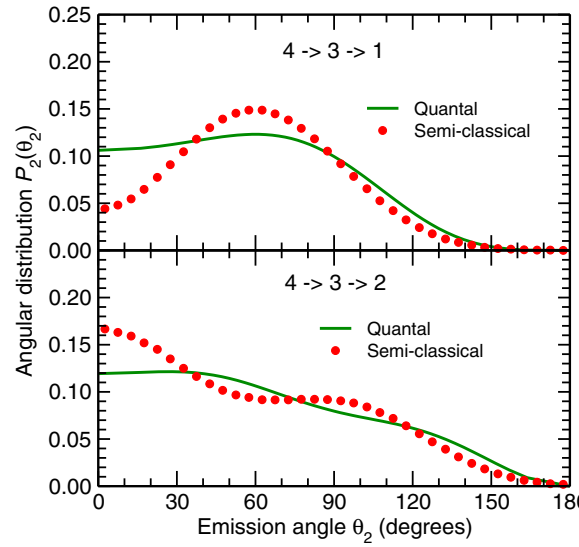

FIG. 5. The angular distribution of the second $E2$ photon, $P_2(\hat{\boldsymbol{\omega}}_2)$, for the two cases where the first $E2$ emission decreases the nuclear-spin magnitude by one unit, $J' = J - 1$, calculated for $h_1, h_2 = 1$. Solid (green) curve: exact distribution; solid (red) circles: semiclassical simulation.

The angular distribution of the first photon is then a mix of $\Delta M = -1$ and $\Delta M = -2$,

$$P_1^{E2:-}(\hat{\boldsymbol{\omega}}_1) \sim \frac{J-1}{J+1} d^2_{1,h_1}(\theta_1)^2 + \frac{2}{J+1} d^2_{2,h_1}(\theta_1)^2, \tag{28}$$

and the expectation value of the daughter spin follows,

$$\underline{J}'_\perp(\theta_1) = -\sqrt{2J-2}\,c_1 c_2, \tag{29}$$

$$\underline{J}'_z(\theta_1) = (J-1)c_1^2 + (J-2)c_2^2. \tag{30}$$

The angular distribution of the second photon in $E2$ cascades where the first emission decreases the nuclear spin by one unit, $J' = J - 1$, is illustrated in Fig. 5. It is apparent from the figure that the semiclassical treatment is far from perfect with regard to the directional distribution of the second photon, especially when comparing with the practically perfect results for $E1$ emissions.

However, it should be kept in mind that emission into the polar regions is suppressed by the geometric factor $\sin\theta_2$ and therefore plays a smaller role. (This comment applies to the distributions shown in Fig. 5 as well as to those shown earlier in Figs. 1 and 3.) This effect is illustrated in Fig. 6 for the two $E2$ cascade types considered here. When viewed from this practical perspective, the discrepancies, although significant, are not overwhelming and it may be expected that the approximate treatment can be useful also for $E2$ cascades.

This expectation is supported by the results for the opening-angle distribution, shown in Fig. 7 for the two $E2$ cascade types where $J' = J - 1$. As can be seen, the semiclassical treatment yields a remarkably good (in fact practically perfect) reproduction of the exact $P_{12}(\psi)$ for the $E2$-$E2$ cascades.

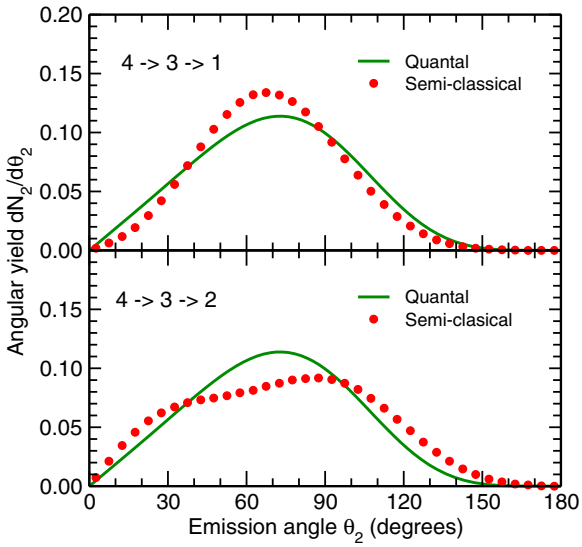

FIG. 6. The angular yield of the second $E2$ photon, $dN_2/d\theta_2 = P_2(\theta_2)\sin\theta_2$, for the two cases where the first $E2$ emission decreases the nuclear spin by one unit, $J' = J - 1$, calculated for $h_1, h_2 = 1$. Solid (green) curve: exact distribution; solid (red) circles: semiclassical simulation.

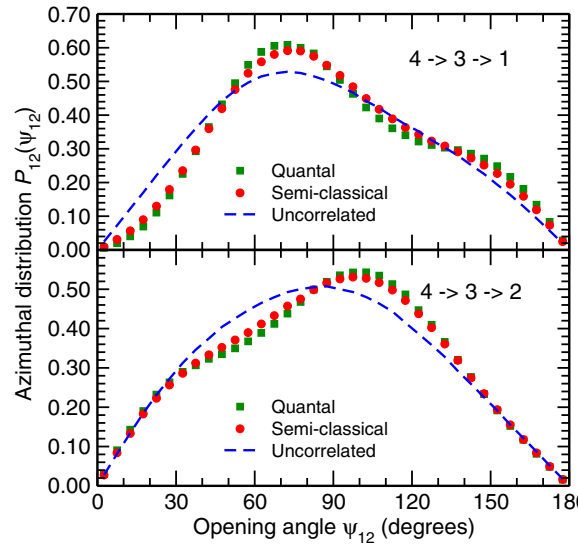

FIG. 7. The distribution of the opening angle between the emission directions of two sequential $E2$ photons, $P_{12}(\psi)$, for the two $E2$ cases where the first emission reduces the nuclear spin by one unit, $J' = J - 1$, calculated for $h_1, h_2 = 1$. Solid (green) squares: sampling of the exact correlated distribution $P_{12}(\hat{\boldsymbol{\omega}}_1, \hat{\boldsymbol{\omega}}_1)$; solid (red) circles: semiclassical sampling; dashed (blue) curve: uncorrelated emission.

Also here it should be noted that the correlated results differ significantly from those corresponding to uncorrelated emissions.

IV. CONCLUDING REMARKS

We have presented a novel semiclassical treatment of photon emission that is particularly well suited for Monte Carlo simulations of decay cascades, such as those occurring in fission fragments.

The key approximation is to represent each fragment by a maximally aligned quantum state, using the direction of its original classical angular momentum as the initial alignment direction and then modifying the alignment direction after each emission depending on the emission direction. The inclusion of this spin recoil effect at each stage of a cascade ensures that the resulting many-photon emission pattern (approximately) retains its inherent correlations.

The quantitative utility of this approximate treatment was illustrated by a variety of two-photon cascades. For $E1$ cascades it was shown that the treatment works very well for both the individual angular distributions and for the distribution of the opening angle between the two photons. For $E2$ cascades the reproduction of the individual distributions is less perfect but still acceptable, while the opening-angle distributions are practically perfectly reproduced.

The developed semiclassical treatment is straightforward to implement into existing fission simulation codes such as FREYA. Because the treatment keeps track of how the fragment angular-momentum vector is affected by each photon emission, the evolution of the correlated spin-spin distribution can be followed through the cascade stage. In particular, the results presented suggest that such an augmentation would make it possible to address the photon correlations in a quantitatively meaningful manner and develop more refined observables for probing the fission-fragment angular momenta.

ACKNOWLEDGMENTS

We thank R. Vogt for helpful discussions. This work was supported in part by the Office of Nuclear Physics in the U.S. Department of Energy's Office of Science under Contract No. DE-AC02-05CH11231.

[1] J. B. Wilhelmy, E. Cheifetz, R. C. Jared, S. G. Thompson, H. R. Bowman, and J. O. Rasmussun, Angular momentum of primary products formed in the spontaneous fission of ^{252}Cf, Phys. Rev. C **5**, 2041 (1972).

[2] A. Wolf and E. Cheifetz, Angular distributions of specific gamma rays emitted in the deexcitation of prompt fission products of ^{252}Cf, Phys. Rev. C **13**, 1952 (1976).

[3] J. Wilson *et al.*, Angular momentum generation in nuclear fission, Nature (London) **590**, 566 (2021).

[4] A. Al-Adili, Z. Gao, M. Lantz, A. Solders, M. Österlund, and S. Pomp, Isomer yields in nuclear fission, EPJ Web Conf. **256**, 00002 (2021).

[5] M. Travar *et al.*, Experimental information on mass-and TKE-dependence of the prompt fission γ-ray multiplicity, Phys. Lett. B **817**, 136293 (2021).

[6] S. Marin, M. S. Okar, E. P. Sansevero, I. E. Hernandez, C. A. Ballard, R. L. Vogt, J. Randrup, P. Talou, A. E. Lovell, I. Stetcu, O. Serot, O. Litaize, A. Chebboubi, S. D. Clarke, V. A.

Protopopescu, and S. A. Pozzi, Structure in the event-by-event neutron-γ multiplicity correlations in ^{252}Cf(sf), Phys. Rev. C **104**, 024602 (2021).
[7] I. Stetcu, A. E. Lovell, P. Talou, T. Kawano, S. Marin, S. A. Pozzi, and A. Bulgac, Angular momentum removal by neutron and γ-ray emissions during fission fragment decays, Phys. Rev. Lett. **127**, 222502 (2021).
[8] S. Marin, E. P. Sansevero, M. S. Okar, I. E. Hernandez, S. D. Clarke, R. Vogt, J. Randrup, V. A. Protopopescu, and S. A. Pozzi, Directional-dependence of the event-by-event neutron-γ multiplicity correlations in ^{252}Cf(sf), Phys. Rev. C **105**, 054609 (2022).
[9] N. P. Giha *et al.*, Correlations between energy and γ-ray emission in ^{239}Pu(n, f), Phys. Rev. C **107**, 014612 (2023).
[10] D. Gjestvang *et al.*, Examination of how properties of a fissioning system impact isomeric yield ratios of the fragments, Phys. Rev. C **108**, 064602 (2023).
[11] G. F. Bertsch, T. Kawano, and L. M. Robledo, Angular momentum of fission fragments, Phys. Rev. C **99**, 034603 (2019).
[12] R. Vogt and J. Randrup, Angular momentum effects in fission, Phys. Rev. C **103**, 014610 (2021).
[13] A. Bulgac, I. Abdurrahman, S. Jin, K. Godbey, N. Schunck, and I. Stetcu, Fission fragment intrinsic spins and their correlations, Phys. Rev. Lett. **126**, 142502 (2021).
[14] P. Marević, N. Schunck, J. Randrup, and R. Vogt, Angular momentum of fission fragments from microscopic theory, Phys. Rev. C **104**, L021601 (2021).
[15] J. Randrup and R. Vogt, Generation of fragment angular momentum in fission, Phys. Rev. Lett. **127**, 062502 (2021).
[16] A. Bulgac, I. Abdurrahman, K. Godbey, and I. Stetcu, Fragment intrinsic spins and fragments' relative orbital angular momentum in nuclear fission, Phys. Rev. Lett. **128**, 022501 (2022).
[17] J. Randrup, T. Døssing, and R. Vogt, Probing fission fragment angular momenta by photon measurements, Phys. Rev. C **106**, 014609 (2022).
[18] J. Randrup, Coupled fission fragment angular momenta, Phys. Rev. C **106**, L051601 (2022).
[19] J. Randrup, Effect of the Coulomb force on fission fragment angular momenta, Phys. Rev. C **108**, 064606 (2023).
[20] T. Døssing, S. Åberg, M. Albertsson, B. Carlsson, and J. Randrup, Angular momentum in fission fragments, Phys. Rev. C **109**, 034615 (2024).
[21] P. Talou *et al.*, Correlated prompt fission data in transport simulations, Eur. Phys. J. A **54**, 9 (2018).
[22] P. Talou, T. Kawano, and I. Stetcu, CGMF: Tech. Rep. LA-CC-13-063, Los Alamos National Laboratory (2013).
[23] P. Talou, I. Stetcu, P. Jaffke, M. E. Rising, A. E. Lovell, and T. Kawano, Fission fragment decay simulations with the CGMF code, Comput. Phys. Commun. **269**, 108087 (2021).
[24] J. M. Verbeke, J. Randrup, and R. Vogt, Fission reaction event yield algorithm, FREYA – For event-by-event simulation of fission, Comput. Phys. Commun. **191**, 178 (2015).
[25] J. M. Verbeke, J. Randrup, and R. Vogt, Fission reaction event yield algorithm FREYA 2.0.2, Comput. Phys. Commun. **222**, 263 (2018).
[26] O. Litaize, O. Serot, and L. Berge, Fission modeling with FIFRELIN, Eur. Phys. J. A **51**, 177 (2015).
[27] K. H. Schmidt, B. Jurado, C. Amouroux, and C. Schmitt, General description of fission observables: GEF model code, Nucl. Data Sheets **131**, 107 (2016).
[28] A. Chalil, T. Materna, O. Litaize, A. Chebboubi, and F. Gunsing, Monte Carlo simulations of γ-directional correlations and their application on FIFRELIN cascades, Eur. Phys. J. A **58**, 30 (2022).